Proceedings of the Second International Workshop on EGS, 8.-12. August 2000, Tsukuba, Japan
KEK Proceedings 200-20, pp.124-129

EGS4 Simulation of the Positron Converter at the BEPC Linac-Based Slow Positron Beam

R. S. Yu, C. X. Ma, G. X. Pei, L. Wei, B. Y. Wang, and T. B. Chang

Institute of High Energy Physics, Academia Sinica
P.O. Box 918, Beijing, 100039, The Peoples Republic of China

Abstract

The Beijing Intense Slow Positron Beam is in the preparation stage of construction. This paper describes the simulations by EGS4 code toward the positron converter and the radiation shield problem. Results show that Beijing Electron-Positron Collider (BEPC) LINAC can produce slow positrons in order of $10^6 - 10^7 e^+/s$ when running under parasitic mode and $10^8 - 10^9 e^+/s$ under dedicated mode.

1 Introduction

In recent years, the interest in the use of slow positron beam as a probe for nuclear physics and solid-state physics has greatly increased. Usually the slow positron beams are created by the re-emission of slow positrons from solid surfaces. Primary fast positrons are usually from a radioactive source or from the target bombarded by a linear accelerator. The former type of facilities is often used, but the slow positron intensity is restricted to $10^7 e^+/s$ by the activity of the available radioactive source. The Linac-based positron source can enable an increase of the slow-positron intensity by more than several orders of magnitude[1, 2, 3].

Utilizing the 1.55 GeV Linac of BEPC, we will start construction of an intense positron beam, aiming to produce about $10^6 - 10^7 e^+/s$ slow positrons when BEPC is running under conventional mode (Mode I, 2.5 ns pulse width, 12.5 pulses/s repetition rate, 1000 mA peak current) and $10^8 - 10^9 e^+/s$ slow positrons under dedicated operation mode (Mode II-in construction, 1.6 μs pulse width, 50 pulses/s repetition rate, 50 mA peak current). As one of the most important parts to obtain the slow positrons, the positron converter should be carefully designed[4, 5]. Since no simple relation exists which correlates the converter thickness to the energy of the impinging electrons, we performed Monte-Carlo simulations as a function of the electron energy and the thickness of the converter to obtain the optimum thickness of the converter. The angular spread and the energy distribution of the outgoing positrons were studied. Detailed calculation about the thermal power distribution as a function of depth and radius of the converter was also performed. Some simulation results toward radiation shield problem are also reviewed in this paper.

2 Simulation Results

The EGS4 code[6] was used on a Windows PC to perform the Monte-Carlo simulations. The geometry of the converter and the radiation shield wall is presented in figure 1. We used tantalum or tungsten as the converter material, which was considered being a cylindrical slab surrounded by vacuum and bombarded by the electron with energy of 1.55 GeV. The electrons were considered at normal incidence and a total of 10000 events were followed. The radiation shield wall is made up of a 0.2 m thick square Fe plate and a 1.8 m thick square concrete wall, which is installed after the

target. The Monte-Carlo process was followed down to energy of 1.02 MeV for electrons, positrons and photons, since there will be no pair production occurring below this energy.

The thickness of the converter was varied between 10 mm and 35 mm for finding the optimal thickness which representing the largest fast positron yield. The relationship between the fast positron yield and the target thickness is shown in figure 2. This figure shows that the optimal thickness is equal to 18 mm and the converting efficiency from the incident electrons to fast positrons equals to about 9.5% for both tantalum and tungsten materials. If the moderation efficiency of the positron moderator located behind the converter equals to 10^{-4}, the slow positron yield will equal to $10^6 - 10^7 e^+/s$ when the BEPC LINAC is running under mode I and $10^8 - 10^9 e^+/s$ under mode II. Figure 3 gives the angular dependence of the outgoing fast positrons. One can see that the fast positrons are peaked in the forward direction. The number of fast positrons as function of the emitting angle decreases very fast. This means that the positron moderator has to be placed as close as possible to the positron converter in order to moderate as much as possible fast positrons.

Figure 4 shows the energy spectrum of the fast positrons out of the 18 mm thick tantalum converter, it has a steep decrease towards lower energies and a long tail towards higher energies. The spectrum is peaked below 10 MeV and there is a small shift for the number of positrons between 5 MeV and 10 MeV.

The thermal power distributions as a function of the injection depth and radius of the converter are shown in figure 5 and figure 6, respectively. For the pencil beam of electrons, the effective radius near showrr maximun is about 0.5 mm. The temperature rises of tungsten target during the effective radius accompanying one beam pulse is approximately

$$\Delta T = \frac{1}{\rho C_P \pi a^2} \frac{dQ}{dzdt} \frac{1}{v} = 29^0 C$$

Where
(ρ)= the density (($\rho = 19.25 g/cm^3$) for tungsten)
(C_P)=the specific heat (0.138 J/g ($^\circ C$) for tungsten)
a=the radius of energy deposition (0.5 mm)
dQ/(dzdt)=the rate of heat deposition
(μ) =the accelerator repetition rate (12.5 pulses/sec)
So, a water-cooled converter, with a water flow of at least 4 (cm^3/s), is crucially required for heat transferring.

Since the electrons are accelerated to an extreme high energy by the LINAC, the radiation shield around the target is another critical technical problem. Simulation results by EGS4 showed that when the length of the square side of the Fe plate and the concrete wall both equal to 1 m, the energy deposited in the tantalum slab, Fe plate and the concrete wall shares 31.2%, 45.7% and 11.2%, respectively. The energy deposited in the outer region (region 3 in fig.1) between the target and the shield wall shares about 11.9%. Total energy deposited outside of the concrete wall (region 6 in fig.1) equals to (1.067×10^{-7}) kW when the LINAC is running under Mode I, which has been supplying a safe operation environment.

3 Conclusion

Detailed simulations toward the converter on the Beijing intense slow positron beam were performed. It has been shown that a realistic number of ($10^6 - 10^7 e^+/s$) slow positrons when BEPC LINAC is running under parasitic mode and ($10^8 - 10^9 e^+/s$) slow positrons under dedicated mode can be produced. Meanwhile, experiment using a real target to confirm the feasibility and test the validity of the above simulations is the future work.

Acknowledgements

This work is supported by the National Natural Science Foundation of China under grant No.19927001 and the Key-project of Chinese Academy of Sciences under grant No. KJ952-S1-416. We are very appreciated to Prof. Hirayama for his kindly help about the EGS code, and other useful information. R. S. Yu acknowledge KEK for financial support. L.Wei would like to thank to Dr. T. Kurihara for useful discussions.

References

[1] R. Ley, Materials Science Forum.**105-110**,1927-1930(1992).

[2] T. Akahae, T. Chiba, N. Shiotani et al., *Appl.Phys. A* **51**(1990)146-150.

[3] T. Kurihara, A. Shirakawa, A. Enomoto, et al., *Applied Surface Science* **85**(1994)178-181.

[4] S. Okada and H. Sunaga, *Nucl. Instr. and Meth. B* **56/57**(1991)604-609.

[5] S. Okada and H. Kaneko, Proceeding of the First International Workshop on EGS4, KEK, Tsukuba, Japan, 302-309(1997).

[6] W. R. Nelson, H. Hirayama and D. W. O. Roger, "The EG4 Code System", *SLAC-265*. Stanford Linear Accelerator Center(1985).

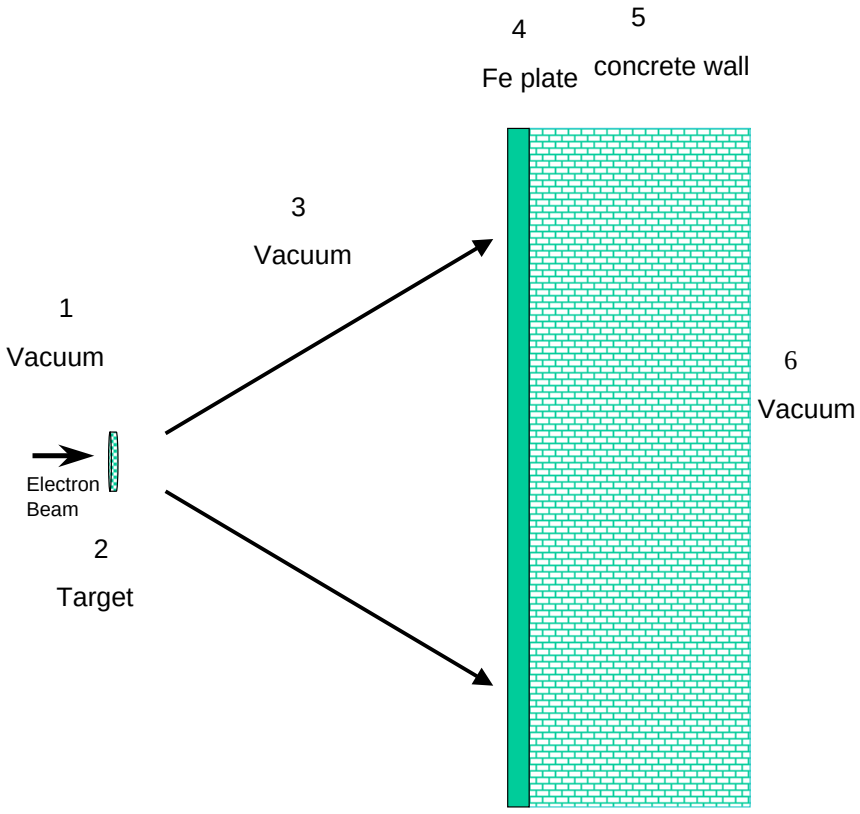

Figure 1: Simulation geometry of the converter and the radiation shield wall.

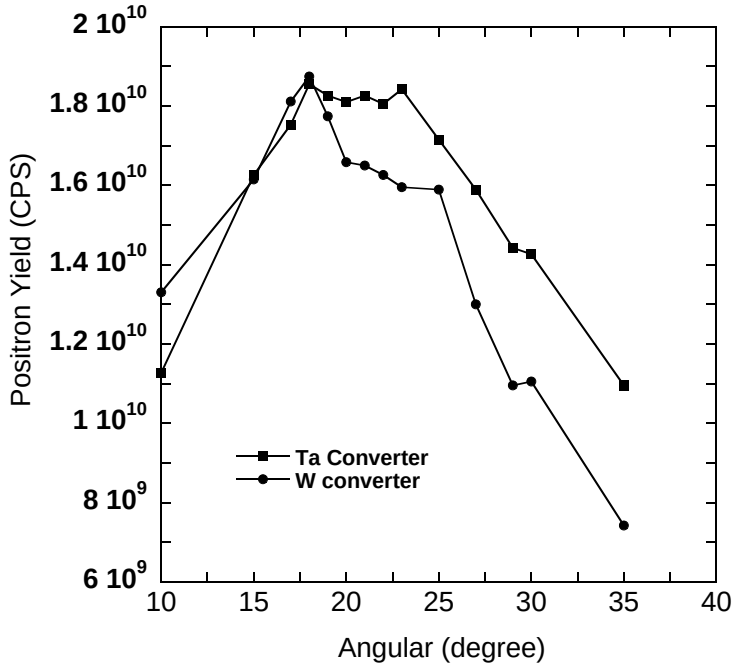

Figure 2: Relationship between the fast positron yield and the target thickness.

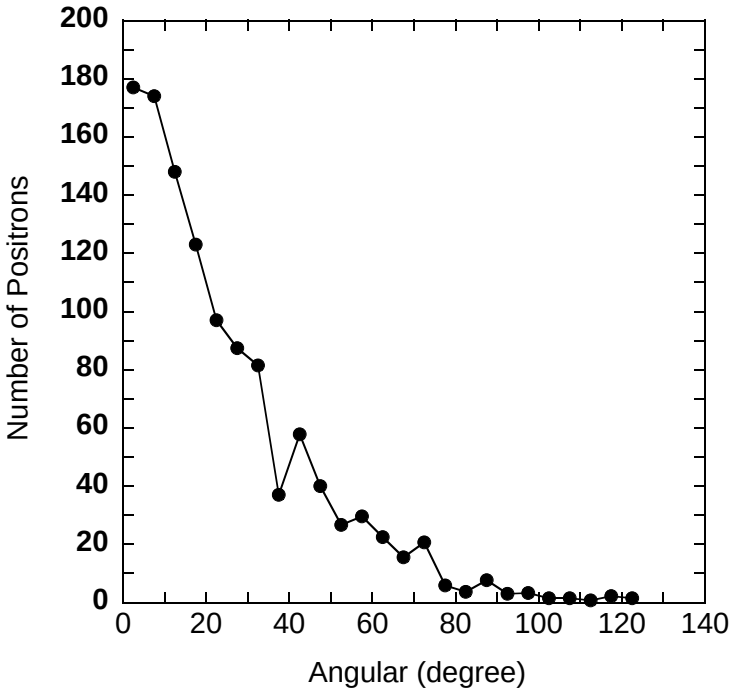

Figure 3: Angular dependence of the outgoing fast positrons.

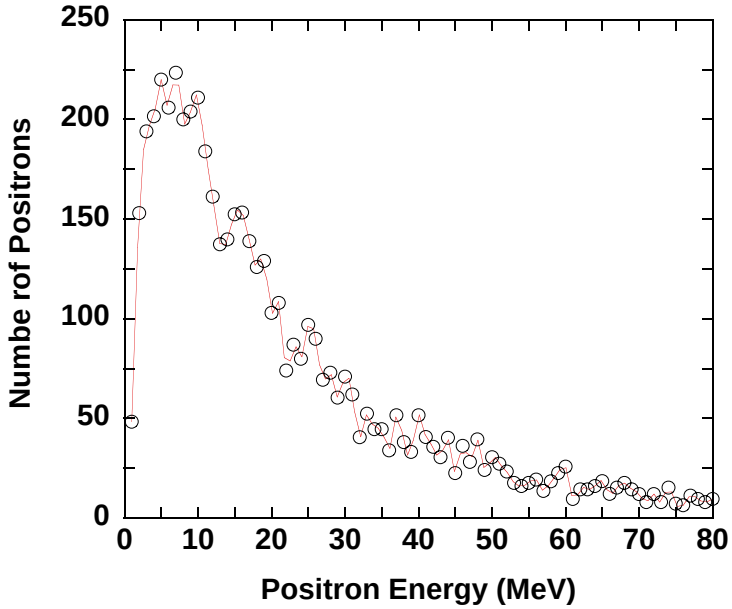

Figure 4: Energy spectrum of the fast positrons out of the 18 mm thick converter.

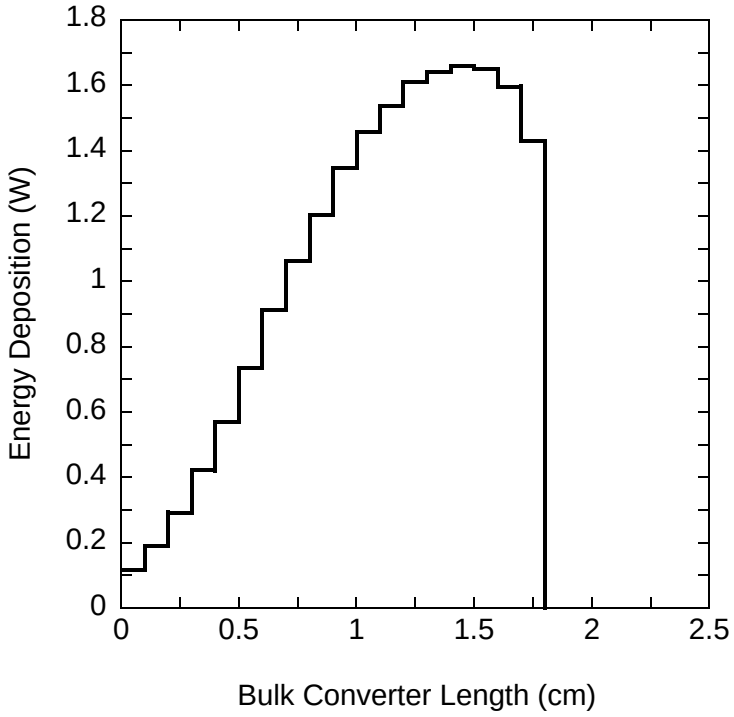

Figure 5: Thermal power distributions as a function of the injection depth.

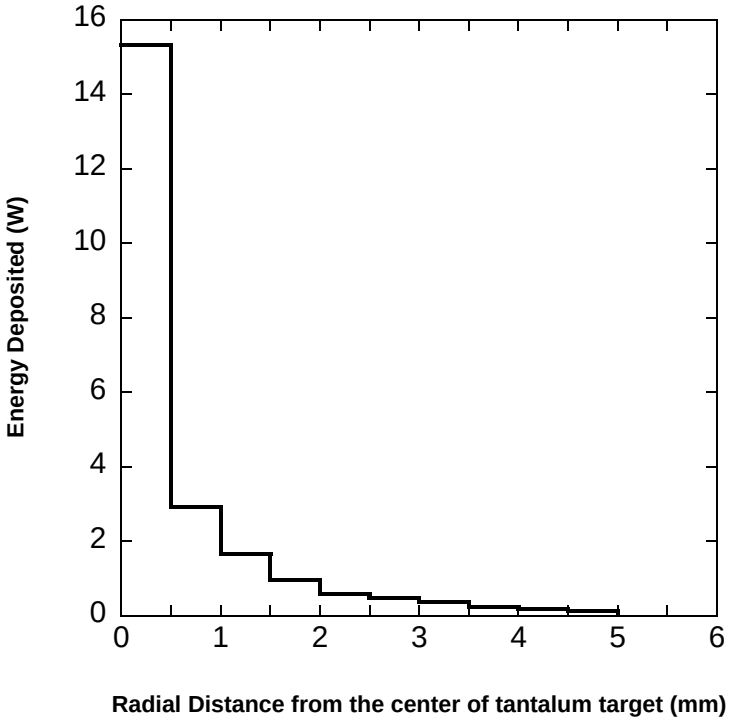

Figure 6: Thermal power distributions as a function of the radial distance.